AD-A273 681

Army Research Laboratory

Correlation of the Failure Modulus to Fracture-Generated Surface Area in Uniaxially Compressed M30 Gun Propellant

— Robert J. Lieb
Michael G. Leadore

ARL-TR-307

November 1993

DTIC
ELECTE
DEC 13 1993
S E D

93-30124

93 12 10 026

NOTICES

REPORT DOCUMENTATION PAGE

Public reporting burden for this collection of information is estimated to average 1 hour per response, including the time for reviewing instructions, searching existing data sources, gathering and maintaining the data needed, and completing and reviewing the collection of information. Send comments regarding this burden estimate or any other aspect of this collection of information, including suggestions for reducing this burden, to Washington Headquarters Services, Directorate for Information Operations and Reports, 1215 Jefferson Davis Highway, Suite 1204, Arlington, VA 22202-4302, and to the Office of Management and Budget, Paperwork Reduction Project(0704-0188), Washington, DC 20503.

1. AGENCY USE ONLY (Leave blank)	2. REPORT DATE November 1993	3. REPORT TYPE AND DATES COVERED Final Nov 92 - Apr 93

4. TITLE AND SUBTITLE

Correlation of the Failure Modulus to Fracture-Generated Surface Area in Uniaxially Compressed M30 Gun Propellant

5. FUNDING NUMBERS

PR: 1L161102AH43

6. AUTHOR(S)

Robert J. Lieb and Michael G. Leadore

7. PERFORMING ORGANIZATION NAME(S) AND ADDRESS(ES)

US Army Research Laboratory
ATTN: AMSRL-WT-PE
Aberdeen Proving Ground, MD 21005-5066

8. PERFORMING ORGANIZATION REPORT NUMBER

9. SPONSORING/MONITORING AGENCY NAMES(S) AND ADDRESS(ES)

US Army Research Laboratory
ATTN: AMSRL-OP-CI-B (Tech Lib)
Aberdeen Proving Ground, MD 21005-5066

10. SPONSORING/MONITORING AGENCY REPORT NUMBER

ARL-TR-307

Accesion For

NTIS CRA&I	☒
DTIC TAB	☐
Unannounced	☐
Justification	

By _____
Distribution /

Availability Codes

| Dist | Avail and / or Special |
| A-1 | |

11. SUPPLEMENTARY NOTES

12a. DISTRIBUTION/AVAILABILITY STATEMENT

Approved for public release; distribution is unlimited.

12b. DISTRIBUTION CODE

DTIC QUALITY INSPECTED 3

13. ABSTRACT (Maximum 200 words)

M30, a triple base large caliber propellant, was uniaxially compressed at a rate of 100/s to an end state strain of 50.0%, 20.0%, and 10.0% at temperatures from -40 to 60 degrees C. The failure modulus was measured, and closed bomb firings were made to determine how the grain damage affected the pressure generation. The pressure-time curves from the damaged propellant were analyzed to extract the burning surface area profiles. Results showed that a line fit to the first 10% of the surface area versus fraction burned curve seemed to be directly related to the logarithm of the failure modulus. The three resulting least square fit curves, one for each level of strain, fell into a series that permitted the effective surface area profile to be predicted for any combination of failure modulus and end state strain within the fracture domain. These results provide a method for assessing fracture damage by means of a simple mechanical measurement.

14. SUBJECT TERMS

mechanical response, surface area, fracture damage, propellants, M30, failure modulus, failure

15. NUMBER OF PAGES

26

16. PRICE CODE

17. SECURITY CLASSIFICATION OF REPORT	18. SECURITY CLASSIFICATION OF THIS PAGE	19. SECURITY CLASSIFICATION OF ABSTRACT	20. LIMITATION OF ABSTRACT
UNCLASSIFIED	UNCLASSIFIED	UNCLASSIFIED	SAR

Intentionally Left Blank

TABLE OF CONTENTS

Intentionally Left Blank

LIST OF FIGURES

LIST OF TABLES

Intentionally Left Blank

1. INTRODUCTION

Attempts to establish the relationship between mechanical measurements and gun performances have made steady progress in the past 5 years[1-13]. Early work revealed that conventional mechanical parameters did not relate well to fracture susceptibility. The search for a simple mechanical parameter that could measure the propensity of a propellant to generate surface area upon mechanical failure resulted in the development of a failure parameter called the failure modulus[4], E_f, that measures the rate at which the material strength is lost as a function of strain, after failure has occurred. This parameter has been used as a guide in the development of new propellants to ensure that improvements in formulation and processing did not degrade the mechanical response characteristics of the material, which could result in poor performance and increased vulnerability response. This parameter has also been successfully used to evaluate the relative fracture susceptibility among several propellant lots or between unconditioned propellant and propellant that has been subjected to conditioning, such as thermal cycling, that may affect its mechanical response.

This parameter showed indications of direct usefulness when the changes of the vulnerability response related directly to the changes measured in this failure parameter[3]. The correlation was found for propellant beds at low temperature subject to a shaped charge jet attack and led to other studies that attempted to make the correlation more direct. However, the relationship was made between changes in both responses, rather than directly relating the responses themselves.

In this study, a direct link between this parameter and a measure of the amount of fracture-generated surface area produced during uniaxially compression is made for M30 propellant. Measurement of the failure modulus was made on the grains, and enough grains were damaged so that closed bomb firings could be made to determine how the grain damage affects the pressure generation under ballistic pressures. A small (21 cc) closed bomb was used so that large numbers of grains did not have to be damaged to reach gun-like pressures in the closed vessel. After the burning rate using undamaged grains was established, the pressure-time curves from the damaged propellant were analyzed for surface area. Many attempts were made to establish a method for analyzing the closed bomb data. As proper considerations became clearer, modifications of the analysis were made, which resulted in a method that relates the augmentation of pressure generation to the failure modulus and the level of strain suffered by the M30 propellant.

The question of the use of uniaxial response measurements to link a mechanical parameter of a propellant grain to the aggregate behavior within gun systems must be addressed. Certainly, the system is complex and the system elements are nonlinear. The success of linking a simple testing
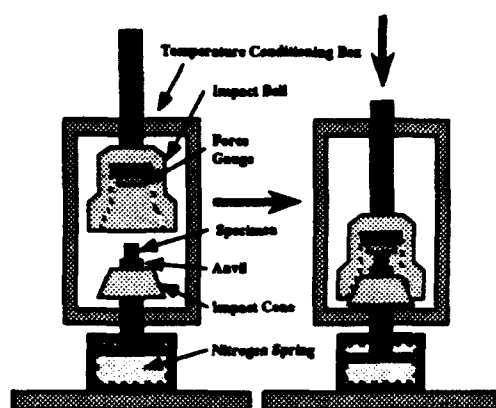
1

Figure 1. Servohydraulic Tester

Table 1. M30 Nominal Percent Composition

Component	Percent Composition
Nitrocellulose (NC)	28
NC Nitration Level	12.6
Nitroglycerin (NG)	22
Nitroguanidine (NQ)	48
Ethyl Centralite (EC)	2

procedure to a complex event will depend upon the ability to extract from the uniaxial response an essential indicator of fracture behavior within the system. As of yet, this has not been demonstrated. However, indications are from the examples cited above that the propellant response seems robust enough to provide some guidance for using these measurements as such an indicator. Attempts are under way to link the grain and aggregate mechanical response in a way to predict bed behavior from grain response and size. As more information is extracted from the response measurements, the ability to predict will become clearer.

2. EXPERIMENTAL PROCEDURE

2.1 Mechanical Response Measurement The propellant response was measured using a specially designed servohydraulic tester[5], illustrated in Figure 1. The machine allows for compression measurements to be performed at rates as great as 1000 s⁻¹ for a specimen with a nominal length of 1 cm. Compression is arrested when contact occurs between the impact bell and cone. Therefore, the amount of specimen compression can be accurately predetermined by setting the anvil height. This contact between bell and cone not only stops the specimen compression, but it also shunts the force around the specimen. The nitrogen spring absorbs the decelerating force of the massive ram and and extends its duration. The force applied to the specimen is measured using the gauge inside the impact bell. During compressive response measurements, displacement is measured with a linear variable differential transformer (LVDT) in the actuator column and is corrected for machine stiffness.

The specimens were prepared from multiperforated M30 gun propellant grains whose formulation is listed in Table 1. Specimen preparation procedure began by cutting the sample with a diamond saw to a length of 1.00 cm. The ends were cut flat, parallel and perpendicular to the grain axis according to the specifications in a proposed NATO draft Standard Agreement entitled "Uniaxial

2

Compressive Test," which is an updated version of the test entitled "Uniaxial Compressive Gun Propellant Test" in the Chemical Propulsion Information Agency Publication 21. Temperature conditioning was achieved by placing prepared grains inside the environmental chamber for a time at least twice that needed to reach thermal equilibrium (30 minutes in most cases). The specimen was then placed on the anvil and tested. This testing took place within the conditioning chamber, so no transfer was required, and therefore, no thermal disruption occurred.
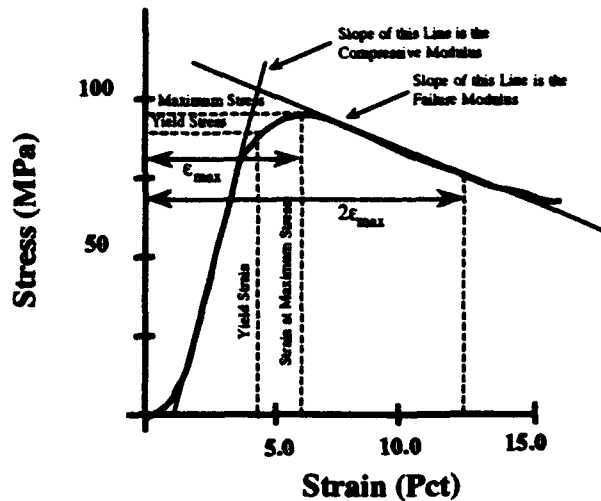

Figure 2. Mechanical Characterization Parameters

The final strain to which the specimen was taken was determined by the distance between the anvil and the force gauge when the bell and cone surfaces were mated. That distance was determined by placing a lead specimen on the anvil and performing a compression. This allowed for any dynamic effects to be taken into account that may have been overlooked in a static measurement. The percentage strain used in these tests was selected to be 50%, 20%, and 10%. From previous testing, it is known that failure of the grain occurs between 3% and 5%, depending upon strain rate and temperature.

The parameters measured in a response characterization test are the modulus, maximum stress, strain at maximum stress, stress at failure, strain at failure, and failure modulus. These parameters are illustrated in Figure 2. The failure modulus is the slope of the stress-strain curve in the near linear region between strain at maximum stress, and twice that value. If no maximum stress occurs in the region of failure, the failure modulus is measured between the strain at failure and three times that value. Measurement of the failure modulus was made at -40°C, -20°C, 0°C, 20°C, 40°C, and 60°C, and the reported values were determined from the average of five response curves. The specimen strain rate was chosen to be 100 s⁻¹, which is the order of strain rate encountered by the grains during a normal ballistic firing.

2.2 Fracture-Generated Surface Area Measurement The grains that were damaged by uniaxial compression, as outlined above, were burned in a mini-closed bomb (MCB) to determine the effect that the mechanical damage had on the pressure generation of the propellant. The MCB is a special, small volume closed bomb[6]. The rate of pressurization during combustion is controlled by the

3

intrinsic burning rate of the propellant and the surface area exposed to the flame. This enables the surface area to be determined once the burning rate of the propellant has been established.

Undamaged specimens were burned in the MCB at the same loading density that was used in the damaged grain firings. These pressure-time traces were analyzed using the closed bomb reduction code BRLCB[14] to establish the burning rates for the M30 propellant for these tests. Once established, the surface area from all the pressure-time histories can be determined using the same code. The output from the code provides pressure in MPa and the corresponding surface area in square centimeters. This output was converted to intrinsic parameters of fraction burned and surface area ratio (S/S_0), respectively, by dividing the pressure by the maximum pressure and the surface area by the initial surface area of the undamaged grain. This permitted closed bomb runs with different charges, pressures, etc., to be compared.

2.3 Details of the Experiment Enough grains were damaged to provide two or three closed bomb firings for each temperature-strain condition. Initial tests done at 50% strain had three repetitions performed. Indications from that set of tests were that two closed bomb firings could be performed with reasonable assurance of agreement. If results varied significantly, subsequent tests were performed to resolve the differences. With six temperatures and three end-strain conditions, a total of 46 closed bomb tests were conducted. These included some instances when more that three firings were performed to verify the repeatability of the process.

3. RESULTS

The uniaxial compressive mechanical response of M30 propellant is shown in the stress vs. strain curves presented in Figure 3. From these curves, the failure modulus was calculated as outlined above. The resulting values of failure modulus are shown in Figure 4 in which the natural logarithm (ln) of these values is plotted against temperature to show the nature of the response. From these plots, the indication is that fracture becomes rapidly more significant at lower temperatures. This was confirmed by the physical appearance of the grains after testing. Figure 5 shows typical 50% strain specimens after uniaxial compression. The failure modulus values reflected the increase in fracture observed in the tested specimens, but more importantly, E_f quantified it. This observation prompted the application of this parameter to the characterization of the effect that damage has on the burning of propellant.

For each closed bomb firing, a surface area ratio vs. fraction burned plot was obtained, as described above, which reflected the amount of surface area available to the flame throughout the
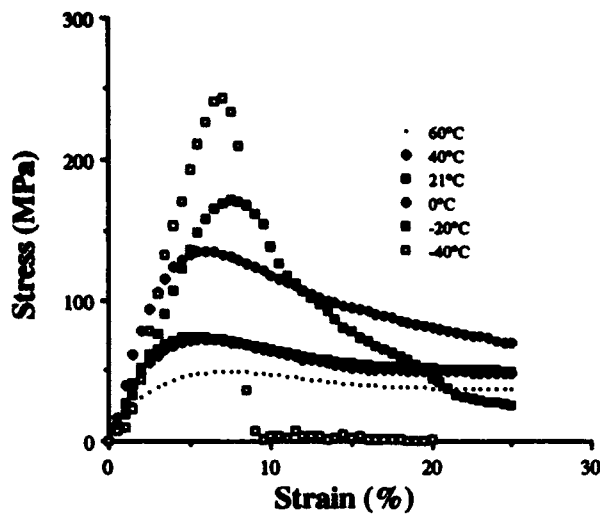
Figure 3. Stress vs. Strain Response Curves for M30 from which Failure Modulus Values are Determined
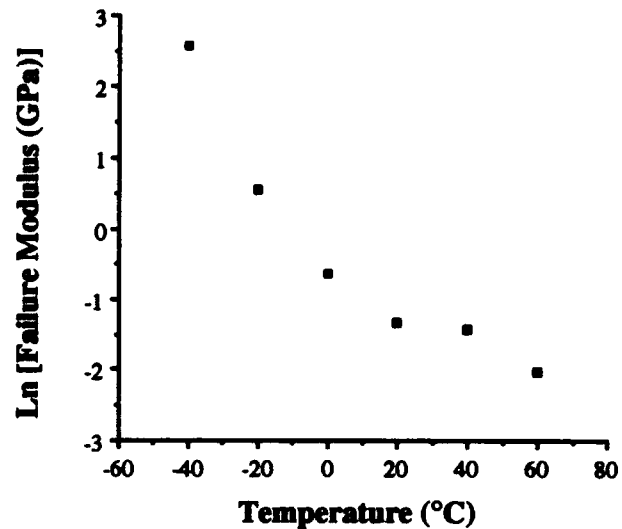
Figure 4. Ln of the Failure Modulus of M30 Propellant vs. Temperature over the Temperature Range of Ballistic Interest
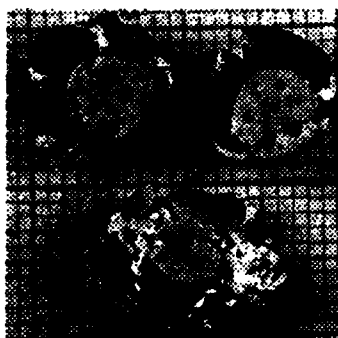

a. -40°C

b. -20°C

c. 0°C

d. 21°C

e. 40°C

f. 60°C

Figure 5. Photographs of the M30 Propellant Specimens after Compression to 50% Strain (1-mm Divisions)
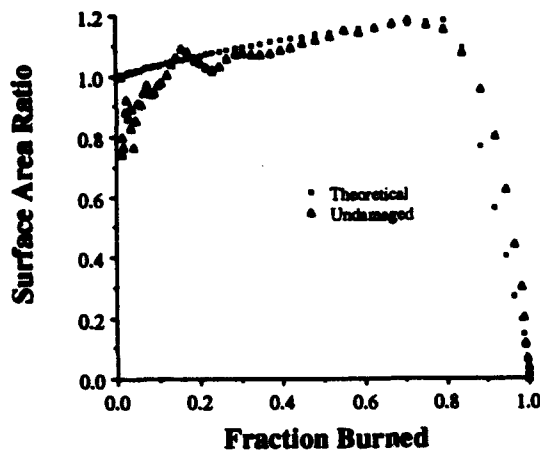
Figure 6. Theoretical and Undamaged Values of the Surface Area Ratio vs. Fraction Burned
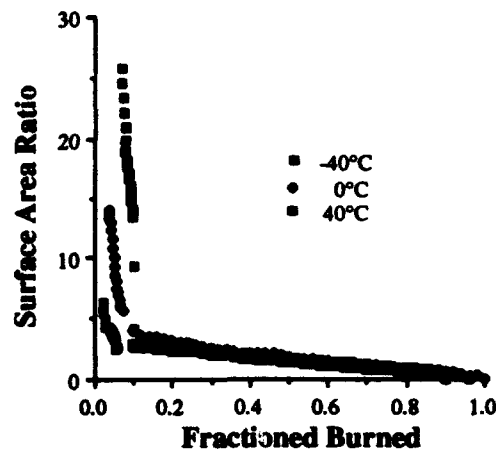
Figure 7. Surface Area Profiles for Propellant Damaged at 50% Strain

propellant combustion. Figure 6 shows the theoretical and typical experimental values for the surface area ratio vs. fraction burned for undamaged grains. Note that as the seven-perforated grains burned, the surface area increased. This area profile is required to provide the gun with the designed performance. Any deviation from this profile changes the performance. In cases of grain fracture, the performance is almost always reduced and, in cases of extensive damage, can produce catastrophic gun failure. The surface area profiles shown in Figure 7 show how temperature and strain combine to change the pressure generation because of damaged grains. These deviations from the profile required for efficient gun firing are significant and would cause large pressure variations within the gun. The profiles for each condition were analyzed using the procedure outlined below.

4. ANALYSIS

4.1 Statement of the Problem Many attempts were made to associate the surface area curves obtained from the closed bom⸍ results to the failure modulus. In the first attempt, the intercept of the initial values of S/S$_0$ was used and difficulty was found with the values determined from this approach. Figure 8a illustrates the problem. Here, the intercept of the initial values is shown for two curves that were obtained under drastically different conditions. The curves show that brittle fracture occurred in each case, but the extent of the fracture in the 10% strain test was initially much worse than for the other condition. However, fracture was arrested when compression stopped at 10%. This resulted in many finely fractured particles, because of the increased brittleness at -40°C and a large surface area. However, after the initial burning of the fine particles, the remaining particles had much
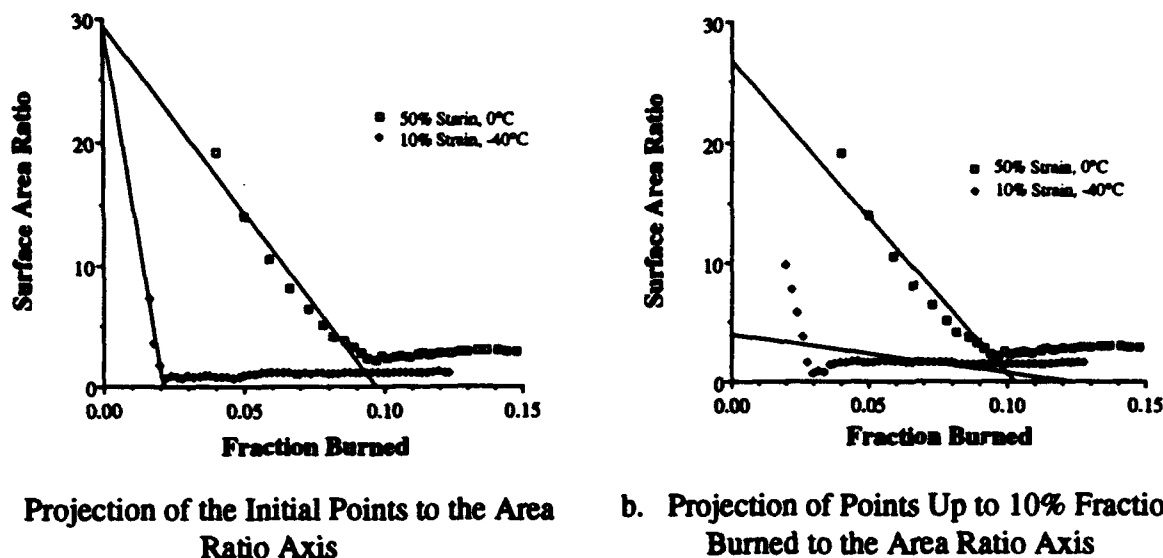
6

a. Projection of the Initial Points to the Area Ratio Axis

b. Projection of Points Up to 10% Fraction Burned to the Area Ratio Axis

Figure 8. S/S$_0$ vs. Fraction Burned for Grains Damaged under Different Conditions

less surface area to present to the flame, and the surface area dropped to significantly lower values at a low fraction burned. The fracture that occurred at 0°C projected the same initial surface area value, but much more extensive damage occurred because of the larger end strain. A much larger mass of finely fractured particles continued to burn rapidly until almost 10% of the charge was consumed. This condition represents a much more rapid rise in pressure and a much greater deviation in the designed surface area profile. A simple method of accounting for the extent of fracture damage needed to be incorporated into the analysis if it was to reflect not only the initial value of the additional fracture-generated surface area, but also the mass and distribution of the fractured particles.

If information outlined above could be reliably extracted from the individual S/S$_0$ vs. fraction burned curves, then a link could be established to ballistic performance. Many attempts were tried: curve averaging, a comparison of areas under curves to a certain fraction burned, shifting of curves to match minimum surface area values, primary and secondary S/S$_0$ curve intercepts, and several other methods. Some of these methods worked well for a particular set of conditions (e.g., constant temperature, or constant end-strain) but failed when applied to the general set of fracture conditions. Much work, which is not detailed here, was done to develop a simple procedure for data analysis. The method that seemed to best characterize the deviation reflected in the curves and was still simple enough to be applied easily is described below.

7

4.2 Method of Analysis As explained above, the initial amount of surface area present is important, and the extent to which that surface area continues to be maintained while the propellant burns is at least as important. It would be desirable to incorporate into a single set of quantitative numbers the degree of pressure generation deviation that can be expected because of fracture damage. To date, the method that best exhibits this information for the conditions used in these tests is to fit the points, to 10% fraction burned, of the S/S_0 vs. fraction burned curve to a least squares fit. If this is performed on the curves in Figure 8a, the intercepts shown in Figure 8b result. Note that the intercept values and the slopes of the curves now seem to reflect a more accurate representation of the effect that the available surface area had on pressure generation.

There are several reasons why this approach reflects critical aspects of pressure generation within the gun. First, the conditions during which significant deviations from planned pressure generation within guns occurare established very early in the ballistic cycle. Thus, it makes sense to use only the information contained in the early burning of the charge, i.e., the first 10%. If surface area variances begin to occur later in the cycle, the performance will be affected, but the chamber volume has increased significantly and is continuing to rapidly expand so that excess pressurization is more difficult to generate than at earlier times. Next, this method also increases the number of points that determine the value to be used to characterize the increased surface area. Those familiar with closed bomb analysis know that the most uncertain values generated in the process are those obtained at low fraction burned. This method of curve fitting eliminates the dependence of the values obtained from being determined by a only few points that lie within the early, uncertain region of fraction burned. However, this early combustion region still is able to influence the parameter values. Finally, by incorporating the points at higher fraction burned (i.e., As great as 10%) the degree by which the fracture-generated surface area is maintained is also taken into account. All these features are exhibited in the examples shown in Figure 8.

4.3 Results of Analysis The above analysis procedure was applied to each of the closed bomb data sets. However, to provide equal weight to each portion of the curve between the points being fit, values of S/S_0 were calculated at equal intervals of fraction burned, i.e., $\Delta FB = 0.02$, based on an interpolation between nearest data points. This was necessary because at high surface area, more propellant is consumed per time interval. This resulted in larger fraction burned intervals at lower fraction burned, or a greater density of points within the curve at higher fraction burned. This higher density skewed the weighting of the fitted curve. This procedure also facilitated curve averaging. The specific surface area at each fraction burned for each curve, at the same end-strain and temperature condition, was averaged between the maximum value of S/S_0 and the value of S/S_0 at

8

0.10 fraction burned. This produced an average curve for that testing temperature and end strain combination. These average curves and the associated least squares fit straight line appear in Figure 9. The intercept and slope values for these lines appear in Table 2 along with the corresponding values of the failure modulus.

If these intercept and slope values are plotted against the logarithm of the failure modulus for each of the end-strain levels, and a linear least squares fit is made to the points, the curves in Figure 10 result. The curves form a series that can be related to the end-strain level by setting the constants and coefficients in the fitting equations to be functions of the end strain. This is done in Figure 11, which shows that the dependence of the fitting parameters on the strain appears to be linear. If the equations shown in Figure 11a are substituted into the relationships developed in Figure 10a, the S/S₀ curve intercept can be represented by

$$S_i/S_0 \ (\varepsilon, E_f) = -1.84 + 0.361 \ \varepsilon +$$
$$(0.392 + 0.116 \ \varepsilon) \ln E_f, \qquad (1)$$

which can be u ⋅d to predict values of effective initial surface area ratio, given the measured failure modulus and the strain.

A similar result can be obtained for the slope of the S/S₀ vs. fraction burned curves. These values also appear in Table 2 and are plotted in Figure 11b. When the same operation is performed on the constants and coefficients of the equations in Figure 10b, the coefficient of the
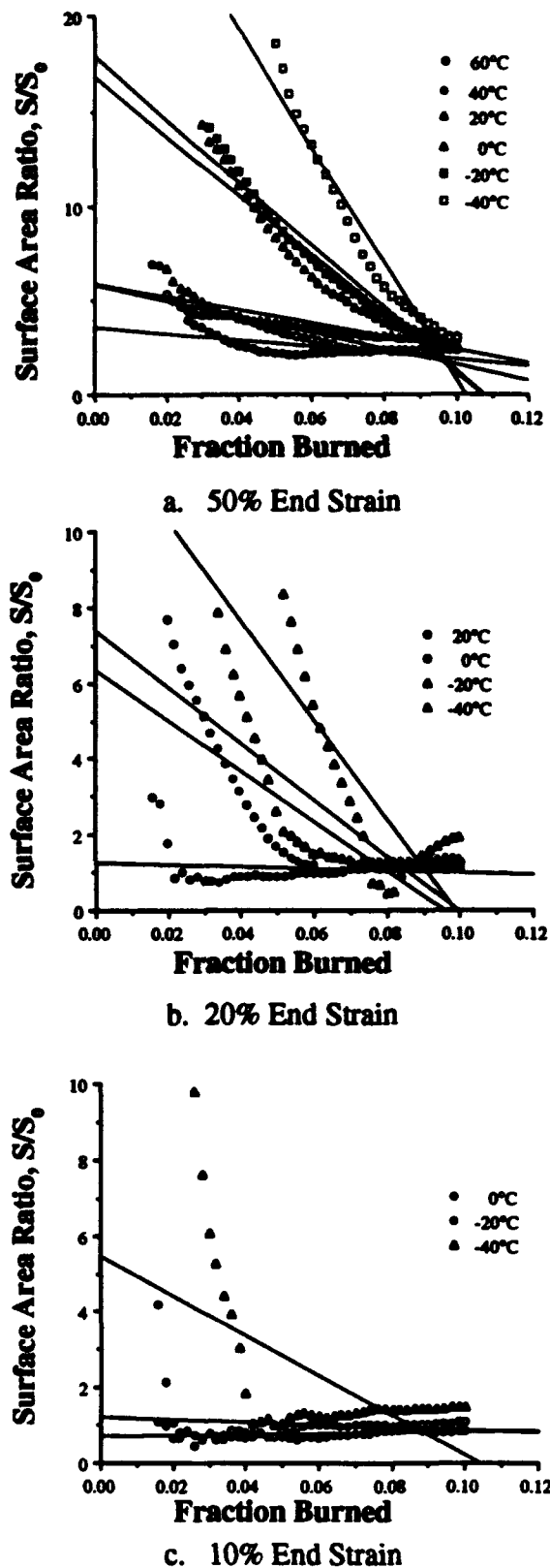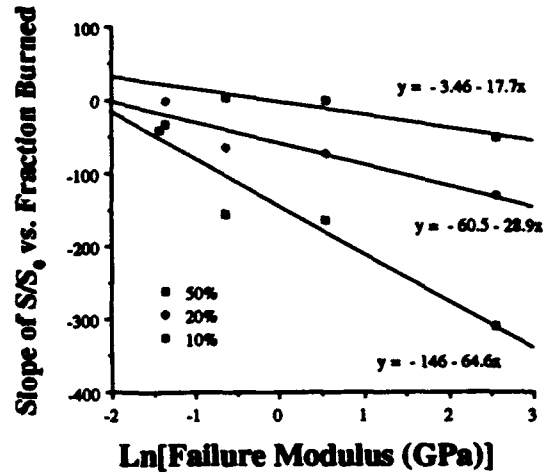

a. 50% End Strain

b. 20% End Strain

c. 10% End Strain

Figure 9. Average S/S₀ vs. Fraction Burned Curves with Least Squared Best Fit Lines

9

Table 2. Average Values of Failure and Surface Area Ratio Parameters

Temperature (°C)	Failure Modulus (E_f) (GPa)	Ln (E_f)	Average S/S₀ Intercept			Average Slope		
			50%	20%	10%	50%	20%	10%
60.0	0.13	-2.040	3.57	-	-	-16.5	-	-
40.0	0.24	-1.427	5.82	-	-	-42.5	-	-
20.0	0.26	-1.347	5.88	1.26	-	-35.0	-2.9	-
0.0	0.53	-0.635	16.80	6.33	0.67	-157	-66.4	1.48
-20.0	1.74	0.554	17.90	7.37	1.20	-166	-74.1	-3.22
-40.0	12.90	2.557	31.80	12.94	5.41	-310	-131.2	-52.6
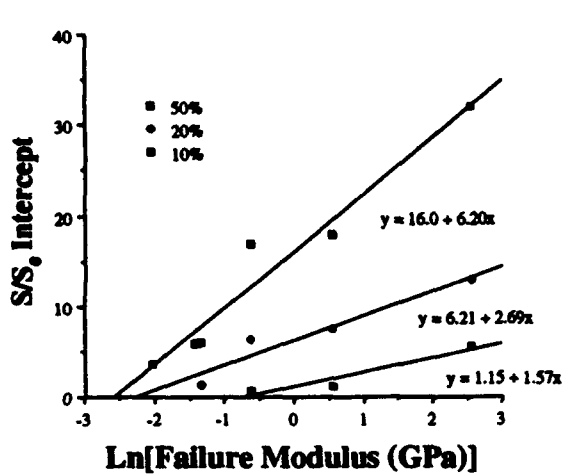
a. Surface Area Ratio Intercept   b. Coefficient of Fraction Burned (Slope)

Figure 10. Least Squares Fit Parameters vs. Ln of the Failure Modulus
of S/S₀ vs. Fraction Burned for Each Strain

effective surface area curve can be found by placing the appropriate end-strain and failure modulus values in the following equation:

$$\text{Slope } (\varepsilon, E_f) = 20.6 - 3.40\,\varepsilon - (5.71 + 1.18\,\varepsilon)\ln E_f. \tag{2}$$

These two equations can be combined to produce the effective surface area profile vs. fraction burned (usually designated as Z) for the first 10% of the fraction burned. This equation appears below:

$$
\begin{aligned}
S/S_0\,(\varepsilon, E_f, Z) &= Si/S_0\,(\varepsilon, E_f) + \text{Slope }(\varepsilon, E_f)\,Z \\
&= -1.84 + 0.361\,\varepsilon + (0.392 + 0.116\,\varepsilon)\ln E_f + \\
&\quad\; [20.6 - 3.40\,\varepsilon - (5.71 + 1.18\,\varepsilon)\ln E_f]\,Z. \tag{3}
\end{aligned}
$$

10

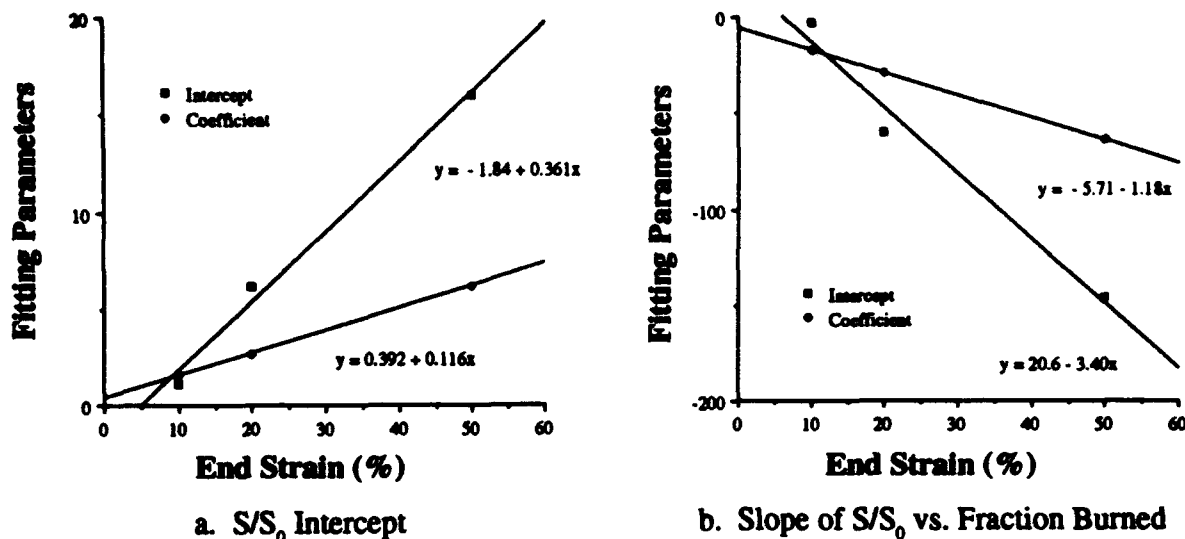a. S/S₀ Intercept   b. Slope of S/S₀ vs. Fraction Burned

Figure 11. Parameters from Fitting Equations in Figure 10 vs. End Strain

The domain over which these relationships can be expected to apply extends a little beyond the corresponding values for ε and E_t for which intercept and slope have been determined in Table 2. The limiting influence is the inability to detect fracture at combinations of low strain and low failure modulus values. There is a greater likelihood of valid results from calculations outside this domain for higher values of ε and E_f.

5. DISCUSSION

5.1 Use of Equations The above equations can be used for several purposes. As stated, if the stress state of the propellant is known and the failure modulus has been measured, then the effect of the initial surface area can be evaluated. The effects of the augmented surface area on combustion for the first 10% of fraction burned can be evaluated by using Equation 3 to predict an effective surface area profile during the early combustion. The prediction may not, however, show the dynamic surface area profile that could affect the generation and propagation of pressure waves within the gun chamber, but it should provide a more accurate assessment of the pressures generated.

Another use of these equations could be to predict when conditions indicate that the fracture-generated surface may become a significant problem. The time-temperature equivalence of M30 and other propellants has been established[10] over the temperature range of ballistic interest and has been related to the strain rate for more than four orders of magnitude[11]. Using this information, one can predict the strain state of a propellant for a certain strain rate deformation at a particular temperature. In the referenced studies, it was shown that the time-temperature equivalency could be extended to

11

predict the failure modulus, as well. This allows for an estimate of the degree of damage and its effect on combustion for a wide variety of conditions, even those outside the area of possible physical measurement. If ballistic codes are used to show when certain surface area profiles subject a system to unacceptable performance, these equations can be used with the appropriate mechanical response parameters to predict when and where these conditions are likely to arise.

Other uses will become evident as the application or problem becomes more well defined. For a long time, the modeling community has had to rely on relatively arbitrary surface area augmentation algorithms. Now, for the first time, a method is available that relates a relatively easily determined mechanical parameter to a surface area profile during the early phase of combustion.

5.2 Observations from Low Fracture Results The experimental results for conditions in which the early grain deformation did not produce evidence of significant fracture during the early fraction burned were not included in the determination of the above equations. There were five such conditions and they are indicated by dashes in Table 2. However, those results did reveal interesting surface area profiles that were consistent with the data thus far reported and offer additional insight about the fracture process within the grains. The profiles that correspond to those five conditions, plus one other profile (20°C and 20% end strain) are shown in Figure 12.

At higher temperatures and lower end strains, most of the deformation is plastic. This is reflected in Figure 12a by surface area values that are smaller than for undamaged grains. This type of surface area reduction has been observed in JA2 propellant that was uniaxially deformed in a completely plastic manner[13]. It is caused by the change of grain dimensions during propellant flow that resulted in less surfacebeing made available to the flame. This can occur by an outright reduction in surface area or by perforations becoming blocked or pinched, thereby delaying the introduction of flame to that portion of the grain. Either mechanism reduces the progressivity of the grain. The profiles in this figure are for the 10% end-strain condition and at 60°C and 40°C, appear about the same. However, the 20°C profile shows a slightly higher profile for low fraction burned and lower progressivity as burning proceeded. This indicated that while plastic deformation was still the predominant failure mechanism, failure by fracture was beginning to influence the profile.

This is demonstrated more clearly in the 20% end-strain profiles in Figure 12b. Here, the loss of progressivity and the increase in available surface area (at 20% fraction burned) was marked. The onset of brittle fracture is indicated at 20°C by the large initial surface area, but the amount of fractured material was small as indicated by the immediate decrease in area. These three curves show that even though a large amount of fracture-generated surface area was not initially available to the

12
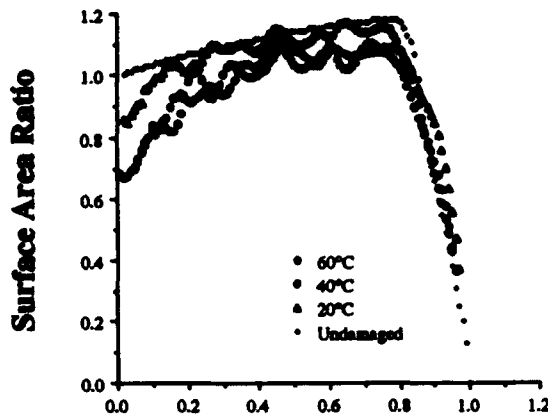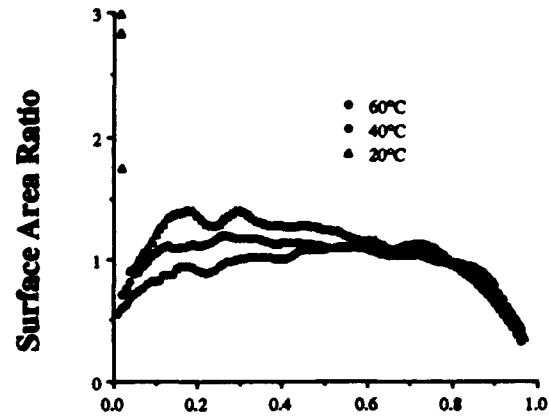
a. 10% End Strain   b. 20% End Strain

Figure 12. Surface Area vs. Fraction Burned for M30 Propellant with Low Fracture Response

flame, fracture surface area soon became available as combustion proceeded. This can occur through crack precursors creating cracks or the uncovering of existing fracture-damaged regions within the grain as the grain burns. In either case, the degree of fracture-related damage was increasing as temperature decreased and end strain increased, even before the grains displayed massive physical fracture. Figure 13 shows two typical grains that were compressed to 20% strain at 20°C. These grains show that the extent of visible fracture damage was small. Even so, the area profile showed the effects of increasingly brittle behavior.

Figure 13. M30 Propellant Grains Compressed to 20% Strain at 20 °C (1-mm Divisions)

6. CONCLUSIONS

A correlation has been established that relates fracture-generated surface area to a mechanical parameter called the failure modulus and the end-state strain of uniaxially compressed propellant grains. The failure modulus has been shown in other studies to demonstrate a time-temperature equivalency that expands the application of these results to a wide variety of ballistic problems.

The effective surface area profile has been shown to be directly proportional to the logarithm of the failure modulus for each of the end-strain conditions tested, and the parameters determined in

these linear correlations (the constant and coefficient of each relationship) have been shown to be linear functions of the strain. The result of this is a method by which an equivalent surface area profile can be generated, based on the level of strain and the established failure modulus. It was also shown that the fracture process can have a demonstrated effect on the surface area profile even when most of the damage is from plastic flow. At high temperatures and low end strains, plastic deformation reduced the specific surface area. As more fracture damage occurs, the profile shows greater area available at low fraction burned and less progressivity. These results have wide application in the modeling and propellant development communities.

7. FUTURE STUDIES

This is the first propellant to undergo this series of tests. To verify the conclusions reached here, the test sequence should be repeated at other strains to see how those results compare with the ones presented here. If the conclusions are affirmed, similar methods of determination should then be performed for the three other major groups of propellants, i.e., single and double base propellants, and the nitramine composite formulations. This, along with the time-temperature equivalency established for each of these groups, should provide a valuable tool to predict the augmentation of pressure generation attributable to fracture damage in ballistic systems.

8. REFERENCES

1. Keller, G. E., and A. W. Horst. "The Effects of Propellant Grain Fracture on the Interior Ballistics of Guns." BRL-MR-3766, USA Ballistic Research Laboratory, Aberdeen Proving Ground, MD, June 1989.

2. Gazonas, G. A., A. Juhasz, and J. C. Ford. "Strain Rate Insensitivity of Damaged-Induced Surface Area in M30 and JA2 Gun Propellants." BRL-TR-3251, USA Ballistic Research Laboratory, Aberdeen Proving Ground, MD, August 1991.

3. Lu, P., B. Strauss, S. Moy, and R. Lieb. "Shaped Charge Jet Impact on Gun Propellants Study I - Temperature and Mechanical Properties Effects," 1991 Propulsion System Hazards Subcommittee Meeting, March 1991.

4. Lieb, R. J., and M. G. Leadore. "Mechanical Failure Parameters in Gun Propellants." BRL-TR-3296, USA Ballistic Research Laboratory, Aberdeen Proving Ground, MD, November 1991.

5. Gazonas, G.A. "The Mechanical Response of M30, XM39, and JA2 Propellants at Strain Rates from 10^{-2} to 250 sec^{-1}." BRL-TR-3181, USA Ballistic Research Laboratory, Aberdeen Proving Ground, MD, January 1991.

6. Lieb, R. J. "Impact-Generated Surface Area in Gun Propellants." BRL-TR-2946, USA Ballistic Research Laboratory, Aberdeen Proving Ground, MD, November 1988.

7. Lieb, R. J. "The Mechanical Response of M30, JA2 and XM39 Gun Propellants to High Rate Deformation." BRL-TR-3023, USA Ballistic Research Laboratory, Aberdeen Proving Ground, MD, August 1989.

8. Lieb, R. J. "High Strain Rate Response of Gun Propellant Using the Hopkinson Split Bar." BRL-TR-3200, USA Ballistic Research Laboratory, Aberdeen Proving Ground, MD, February 1991.

9. Varga, L., and F. Beaupre. "Temperature, Aging and Extrusion Pressure Effects on Mechanical Properties of LOVA Gun Propellants." DREV Memorandum 3072/92, Defence Research Establishment, Valcartier, Quebec, June 1992.

10. Lieb, R. J., and M. G. Leadore. "Mechanical Response Comparison of Gun Propellants Evaluated under Equivalent Time-Temperature Conditions." Proceedings of the 1992 JANNAF Structures & Mechanical Behavior Subcommittee Meeting, CPIA Publication 591, November 1992.

11. Lieb, R. J., and M. G. Leadore. "Time-Temperature Shift Factors for Gun Propellants." ARL-TR-131, Army Research Laboratory, Aberdeen Proving Ground, MD, May 1993.

12. Lieb, R. J., S. F. Trevino, and J. D. Barnes. "Onset and Nature of Fracture of Uniaxially Compressed Gun Propellants, *A Small-Angle Neutron and X-Ray Scattering Study*." ARL-TR-185, Army Research Laboratory, Aberdeen Proving Ground, MD, August 1993.

13. Lieb, R. J., D. Devynck, and J. J. Rocchio."The Evaluation of High Rate Fracture Damage of Gun Propellant Grains." 1983 JANNAF Structure and Mechanical Behavior Subcommittee Meeting, CPIA Publication 388, November 1983.

14. Oberle, W. F., and D. E. Kooker. "BRLCB: A Closed-Chamber Data Analysis Program, *Part I - Theory and User's Manual*." ARL-TR-36, Army Research Laboratory, Aberdeen Proving Ground, MD, January 1993.

No. of Copies	Organization	No. of Copies	Organization
2	Administrator Defense Technical Info Center ATTN: DTIC-DDA Cameron Station Alexandria, VA 22304-6145	1	Commander U.S. Army Missile Command ATTN: AMSMI-RD-CS-R (DOC) Redstone Arsenal, AL 35898-5010
1	Commander U.S. Army Materiel Command ATTN: AMCAM 5001 Eisenhower Ave. Alexandria, VA 22333-0001	1	Commander U.S. Army Tank-Automotive Command ATTN: AMSTA-JSK (Armor Eng. Br.) Warren, MI 48397-5000
1	Director U.S. Army Research Laboratory ATTN: AMSRL-OP-CI-AD, Tech Publishing 2800 Powder Mill Rd. Adelphi, MD 20783-1145	1	Director U.S. Army TRADOC Analysis Command ATTN: ATRC-WSR White Sands Missile Range, NM 88002-5502
1	Director U.S. Army Research Laboratory ATTN: AMSRL-OP-CI-AD, Records Management 2800 Powder Mill Rd. Adelphi, MD 20783-1145	(Class. only) 1	Commandant U.S. Army Infantry School ATTN: ATSH-CD (Security Mgr.) Fort Benning, GA 31905-5660
		(Unclass. only) 1	Commandant U.S. Army Infantry School ATTN: ATSH-WCB-O Fort Benning, GA 31905-5000
2	Commander U.S. Army Armament Research, Development, and Engineering Center ATTN: SMCAR-IMI-I Picatinny Arsenal, NJ 07806-5000	1	WL/MNOI Eglin AFB, FL 32542-5000

Aberdeen Proving Ground

No. of Copies	Organization
2	Commander U.S. Army Armament Research, Development, and Engineering Center ATTN: SMCAR-TDC Picatinny Arsenal, NJ 07806-5000
1	Director Benet Weapons Laboratory U.S. Army Armament Research, Development, and Engineering Center ATTN: SMCAR-CCB-TL Watervliet, NY 12189-4050
1	Director U.S. Army Advanced Systems Research and Analysis Office (ATCOM) ATTN: AMSAT-R-NR, M/S 219-1 Ames Research Center Moffett Field, CA 94035-1000

Aberdeen Proving Ground

2	Dir, USAMSAA ATTN: AMXSY-D AMXSY-MP, H. Cohen
1	Cdr, USATECOM ATTN: AMSTE-TC
1	Dir, ERDEC ATTN: SCBRD-RT
1	Cdr, CBDA ATTN: AMSCB-CII
1	Dir, USARL ATTN: AMSRL-SL-I
5	Dir, USARL ATTN: AMSRL-OP-CI-B (Tech Lib)

18

No. of Copies	Organization

1   Commander
U.S. Army Foreign Science and
    Technology Center
ATTN: AMXST-MC-3
220 Seventh Street, NE
Charlottesville, VA 22901-5396

2   Commandant
U.S. Army Field Artillery Center and
    School
ATTN: ATSF-CO-MW, E. Dublisky
        ATSF-CN, P. Gross
Ft. Sill, OK 73503-5600

1   Commandant
U.S. Army Armor School
ATTN: ATZK-CD-MS, M. Falkovitch
Armor Agency
Fort Knox, KY 40121-5215

1   U.S. Army Research Development and
    StandardizationGroup (UK)
PSC 802 Box 15, Dr. Roy E. Richenbach
FPO AE09499-1500

2   Commander
Naval Sea Systems Command
ATTN: SEA 62R
        SEA 64
Washington, DC 20362-5101

1   Commander
Naval Air Systems Command
ATTN: AIR-954-Tech Library
Washington, DC 20360

4   Commander
Naval Research Laboratory
ATTN: Technical Library
        Code 4410,
          K. Kailasanate
          J. Boris
          E. Oran
Washington, DC 20375-5000

1   Office of Naval Research
ATTN: Code 473, R.S. Miller
800 N. Quincy Street
Arlington, VA 22217-9999

---

1   Office of Naval Technology
ATTN: ONT-213, D. Siegel
800 N. Quincy St.
Arlington, VA 22217-5000

2   Commander
Naval Surface Warfare Center
ATTN: Code 730
         Code R-13,
          R. Bernecker
Silver Spring, MD 20903-5000

7   Commander
Naval Surface Warfare Center
ATTN: T.C. Smith
         K. Rice
         S. Mitchell
         S. Peters
         J. Consaga
         C. Gotzmer
         Technical Library
Indian Head, MD 20640-5000

4   Commander
Naval Surface Warfare Center
ATTN: Code G30, Guns & Munitions Div
        Code G32, Guns Systems Div
        Code G33, T. Doran
        Code E23 Technical Library
Dahlgren, VA 22448-5000

5   Commander
Naval Air Warfare Center
ATTN: Code 388,
         C.F. Price
         T. Boggs
        Code 3895,
         T. Parr
         R. Derr
         Information Science Division
China Lake, CA 93555-6001

1   Commanding Officer
Naval Underwater Systems Center
ATTN: Code 5B331, Technical Library
Newport, RI 02840

1   AFOSR/NA
ATTN: J. Tishkoff
Bolling AFB, D.C. 20332-6448

No. of Copies	Organization	No. of Copies	Organization
1	OLAC PL/TSTL ATTN: D. Shiplett Edwards AFB, CA 93523-5000	2	HQ DNA ATTN: D. Lewis A. Fahey 6801 Telegraph Rd. Alexandria, VA 22310-3398
3	AL/LSCF ATTN: J. Levine L. Quinn T. Edwards Edwards AFB, CA 93523-5000	1	Director Sandia National Laboratories Energetic Materials & Fluid Mechanics Department, 1512 ATTN: M. Baer
1	WL/MNAA ATTN: B. Simpson Eglin AFB, FL 32542-5434		P.O. Box 5800 Albuquerque, NM 87185
1	WL/MNME Energetic Materials Branch 2306 Perimeter Rd. STE 9 Eglin AFB, FL 32542-5910	1	Director Sandia National Laboratories Combustion Research Facility ATTN: R. Carling Livermore, CA 94551-0469
1	WL/MNSH ATTN: R. Drabczuk Eglin AFB, FL 32542-5434	1	Director Sandia National Laboratories ATTN: 8741, G. A. Beneditti P.O. Box 969
2	NASA Langley Research Center ATTN: M.S. 408, W. Scallion D. Witcofski Hampton, VA 23605	2	Livermore, CA 94551-0969 Director Lawrence Livermore National Laboratory ATTN: L-355,
1	Central Intelligence Agency Office of Intelligence Resources Room GA-07, HQS Washington, DC 20505		A. Buckingham M. Finger P.O. Box 808 Livermore, CA 94550-0622
1	Central Intelligence Agency ATTN: J. Backofen NHB, Room 5N01 Washington, DC 20505	2	Director Los Alamos Scientific Lab ATTN: T3/D. Butler M. Division/B. Craig P.O. Box 1663
1	SDIO/TNI ATTN: L.H. Caveny Pentagon Washington, DC 20301-7100		Los Alamos, NM 87544 Battelle ATTN: TWSTIAC
1	SDIO/DA ATTN: E. Gerry Pentagon Washington, DC 21301-7100	2	V. Levin 505 King Avenue Columbus, OH 43201-2693
		1	Battelle PNL ATTN: M.C.C. Bampton P.O. Box 999 Richland, WA 99352

No. of Copies	Organization
1	Institute of Gas Technology ATTN: D. Gidaspow 3424 S. State Street Chicago, IL 60616-3896
1	Institute for Advanced Technology ATTN: T.M. Kiehne The University of Texas of Austin 4030-2 W. Braker Lane Austin, TX 78759-5329
2	CPIA - JHU ATTN: H. J. Hoffman T. Christian 10630 Little Patuxent Parkway Suite 202 Columbia, MD 21044-3200
1	Brigham Young University Department of Chemical Engineering ATTN: M. Beckstead Provo, UT 84601
1	Jet Propulsion Laboratory California Institute of Technology ATTN: L.D. Strand, MS 125/224 4800 Oak Grove Drive Pasadena, CA 91109
1	California Institute of Technology 204 Karman Lab Main Stop 301-46 ATTN: F.E.C. Culick 1201 E. California Street Pasadena, CA 91109
3	Georgia Institute of Technology School of Aerospace Engineering ATTN: B.T. Zim E. Price W.C. Strahle Atlanta, GA 30332
1	Massachusetts Institute of Technology Department of Mechanical Engineering ATTN: T. Toong 77 Massachusetts Avenue Cambridge, MA 02139-4307

No. of Copies	Organization
2	University of Illinois Department of Mechanical/Industry Engineering ATTN: H. Krier R. Beddini 144 MEB; 1206 N. Green St. Urbana, IL 61801-2978
1	University of Massachusetts Department of Mechanical Engineering ATTN: K. Jakus Amherst, MA 01002-0014
1	University of Minnesota Department of Mechanical Engineering ATTN: E. Fletcher Minneapolis, MN 55414-3368
3	Pennsylvania State University Department of Mechanical Engineering ATTN: V. Yang K. Kuo C. Merkle University Park, PA 16802-7501
1	Rensselaer Polytechnic Institute Department of Mathematics Troy, NY 12181
1	Stevens Institute of Technology Davidson Laboratory ATTN: R. McAlevy III Castle Point Station Hoboken, NJ 07030-5907
1	Rutgers University Department of Mechanical and Aerospace Engineering ATTN: S. Temkin University Heights Campus New Brunswick, NJ 08903
1	University of Southern California Mechanical Engineering Department ATTN: OHE200, M. Gerstein Los Angeles, CA 90089-5199

No. of Copies	Organization	No. of Copies	Organization
1	University of Utah Department of Chemical Engineering ATTN: A. Baer Salt Lake City, UT 84112-1194	4	Hercules, Inc. Radford Army Ammunition Plant ATTN: L. Gizzi D.A. Worrell W.J. Worrell C. Chandler
1	Washington State University Department of Mechanical Engineering ATTN: C.T. Crowe Pullman, WA 99163-5201		Radford, VA 24141-0299
		2	Hercules, Inc. Allegheny Ballistics Laboratory ATTN: William B. Walkup
1	AFELM, The Rand Corporation ATTN: Library D 1700 Main Street Santa Monica, CA 90401-3297		Thomas F. Farabaugh P.O. Box 210 Rocket Center, WV 26726
1	Arrow Technology Associates, Inc. ATTN: W. Hathaway P.O. Box 4218 South Burlington, VT 05401-0042	1	Hercules, Inc. Aerospace ATTN: R. Cartwright 100 Howard Blvd. Kenville, NJ 07847
3	AAI Corporation ATTN: J. Hebert J. Frankle D. Cleveland P.O. Box 126 Hunt Valley, MD 21030-0126	1	Hercules, Inc. Hercules Plaza ATTN: B.M. Riggleman Wilmington, DE 19894
2	Alliant Techsystems, Inc. ATTN: R.E. Tompkins J. Kennedy 7225 Northland Dr. Brooklyn Park, MN 55428	1	MBR Research Inc. ATTN: Dr. Moshe Ben-Reuven 601 Ewing St., Suite C-22 Princeton, NJ 08540
1	Textron ATTN: A. Patrick 2385 Revere Beach Parkway Everett, MA 02149-5900	1	Olin Corporation Badger Army Ammunition Plant ATTN: F.E. Wolf Baraboo, WI 53913
1	General Applied Sciences Lab ATTN: J. Erdos 77 Raynor Ave. Ronkonkama, NY 11779-6649	3	Olin Ordnance ATTN: E.J. Kirschke A.F. Gonzalez D.W. Worthington P.O. Box 222 St. Marks, FL 32355-0222
1	General Electric Company Tactical System Department ATTN: J. Mandzy 100 Plastics Ave. Pittsfield, MA 01201-3698	1	Olin Ordnance ATTN: H.A. McElroy 10101 9th Street, North St. Petersburg, FL 33716
1	IITRI ATTN: M.J. Klein 10 W. 35th Street Chicago, IL 60616-3799	1	Paul Gough Associates, Inc. ATTN: P.S. Gough 1048 South St. Portsmouth, NH 03801-5423

No. of Copies	Organization	No. of Copies	Organization
1	Physics International Library ATTN: H. Wayne Wampler P.O. Box 5010 San Leandro, CA 94577-0599	1	Veritay Technology, Inc. ATTN: E. Fisher 4845 Millersport Hwy. East Amherst, NY 14501-0305
2	Princeton Combustion Research Laboratories, Inc. ATTN: N. Mer N.A. Messina Princeton Corporate Plaza 11 Deerpark Dr., Bldg IV, Suite 119 Monmouth Junction, NJ 08852	1	Universal Propulsion Company ATTN: H.J. McSpadden 25401 North Central Ave. Phoenix, AZ 85027-7837
3	Rockwell International Rocketdyne Division ATTN: BA08, J. Flanagan J. Gray R. Edelman 6633 Canoga Avenue Canoga Park, CA 91303-2703	1	SRI International Propulsion Sciences Division ATTN: Tech Library 333 Ravenwood Avenue Menlo Park, CA 94025-3493 Aberdeen Proving Ground
2	Rockwell International Science Center ATTN: Dr. S. Chakravarthy Dr. S. Palaniswamy 1049 Camino Dos Rios P.O. Box 1085 Thousand Oaks, CA 91360	1	Cdr. USACSTA ATTN: STECS-PO/R. Hendricksen
1	Science Applications International Corp. ATTN: M. Palmer 2109 Air Park Rd. Albuquerque, NM 87106		
1	Southwest Research Institute ATTN: J.P. Riegel 6220 Culebra Road P.O. Drawer 28510 San Antonio, TX 78228-0510		
1	Sverdrup Technology, Inc. ATTN: Dr. John Deur 2001 Aerospace Parkway Brook Park, OH 44142		
3	Thiokol Corporation Elkton Division ATTN: R. Willer R. Biddle Tech Library P.O. Box 241 Elkton, MD 21921-0241		

USER EVALUATION SHEET/CHANGE OF ADDRESS

This Laboratory undertakes a continuing effort to improve the quality of the reports it publishes. Your comments/answers to the items/questions below will aid us in our efforts.

1. ARL Report Number ____ARL-TR-307____ Date of Report ____November 1993____

2. Date Report Received _____

3. Does this report satisfy a need? (Comment on purpose, related project, or other area of interest for which the report will be used.) _____

_____

_____

4. Specifically, how is the report being used? (Information source, design data, procedure, source of ideas, etc.) _____

_____

_____

5. Has the information in this report led to any quantitative savings as far as man-hours or dollars saved, operating costs avoided, or efficiencies achieved, etc? If so, please elaborate. _____

_____

_____

6. General Comments. What do you think should be changed to improve future reports? (Indicate changes to organization, technical content, format, etc.) _____

_____

_____

_____

	_____
	Organization
CURRENT	_____
ADDRESS	Name
	_____
	Street or P.O. Box No.
	_____
	City, State, Zip Code

7. If indicating a Change of Address or Address Correction, please provide the Current or Correct address above and the Old or Incorrect address below.

	_____
	Organization
OLD	_____
ADDRESS	Name
	_____
	Street or P.O. Box No.
	_____
	City, State, Zip Code

(Remove this sheet, fold as indicated, tape closed, and mail.)
(DO NOT STAPLE)

DEPARTMENT OF THE ARMY

OFFICIAL BUSINESS